Science of the Total Environment 801 (2021) 149538

Contents lists available at ScienceDirect

Science of the Total Environment

journal homepage: www.elsevier.com/locate/scitotenv

# Nanomaterials induce different levels of oxidative stress, depending on the used model system: Comparison of *in vitro* and *in vivo* effects

Isabel Karkossa [a], Anne Bannuscher [b,c], Bryan Hellack [d,e], Wendel Wohlleben [f], Julie Laloy [g], Miruna S. Stan [h], Anca Dinischiotu [h], Martin Wiemann [i], Andreas Luch [b], Andrea Haase [b], Martin von Bergen [a,j], Kristin Schubert [a,*]

[a] *Department of Molecular Systems Biology, Helmholtz-Centre for Environmental Research - UFZ, Leipzig, Germany*
[b] *Department of Chemical and Product Safety, German Federal Institute for Risk Assessment (BfR), Berlin, Germany*
[c] *Adolphe Merkle Institute (AMI), University of Fribourg, Fribourg, Switzerland*
[d] *Institute of Energy and Environmental Technology (IUTA) e.V., Duisburg, Germany*
[e] *German Environment Agency (UBA), Dessau, Germany*
[f] *Advanced Materials Research, BASF SE, Ludwigshafen, Germany*
[g] *Department of Pharmacy, Namur Nanosafety Centre, University of Namur, Namur, Belgium*
[h] *Department of Biochemistry and Molecular Biology, University of Bucharest, Bucharest, Romania*
[i] *IBE R&D Institute for Lung Health gGmbH, Münster, Germany*
[j] *Institute of Biochemistry, Leipzig University, Leipzig, Germany*

## HIGHLIGHTS

- Reliable *in vitro* test systems are needed to facilitate NM risk assessment.
- Proteomics and metabolomics were applied to provide mechanistic insights.
- Oxidative stress-related effects were opposite in macrophages and epithelial cells.
- Mechanistic differences were observed *in vitro* and *in vivo*.
- Nonetheless, a consistent classification of NMs *in vitro* and *in vivo* was achieved.

## GRAPHICAL ABSTRACT

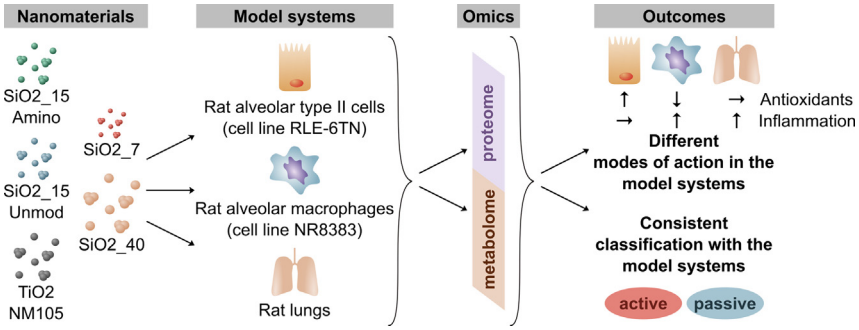


## ARTICLE INFO

*Article history:*
Received 4 March 2021
Received in revised form 3 August 2021
Accepted 4 August 2021
Available online 8 August 2021

Editor: Jay Gan

*Keywords:*
Omics
Mode of action
STIS
Instillation
Alveolar epithelial cells
Alveolar macrophages

## ABSTRACT

The immense diversity and constant development of nanomaterials (NMs) increase the need for a facilitated risk assessment, which requires knowledge of the modes of action (MoAs) of NMs. This necessitates a comprehensive data basis, which can be obtained using omics. Furthermore, the establishment of suitable *in vitro* test systems is essential to follow the 3R concept and to cope with the high number of NMs.

In the present study, we aimed to compare NM effects *in vitro* and *in vivo* using a multi-omics approach. We applied an integrated data analysis strategy based on proteomics and metabolomics to four silica NMs and one titanium dioxide-based NM. For the *in vitro* investigations, rat alveolar epithelial cells (RLE-6TN) and rat alveolar macrophages (NR8383) were treated with different doses of NMs, and the results were compared with the effects on rat lungs after short-term inhalations and instillations.

Since reactive oxygen species (ROS) production has been described as a critical biological effect of NMs, we focused on different levels of oxidative stress. Thus, we found opposite changes in proteins and metabolites related to the production of reduced glutathione in alveolar epithelial cells and alveolar macrophages, demonstrating that the MoAs of NMs depend on the model system used. Interestingly, *in vivo*, pathways related to inflammation were more affected than oxidative stress responses. Hence, the assignment of the observed effects to levels of oxidative stress was also different *in vitro* and *in vivo*.

* Corresponding author at: Department of Molecular Systems Biology, Helmholtz-Centre for Environmental Research – UFZ, Permoserstr. 15, 04318 Leipzig, Germany.
*E-mail address:* kristin.schubert@ufz.de (K. Schubert).

https://doi.org/10.1016/j.scitotenv.2021.149538

However, the overall classification of "active" and "passive" NMs was consistent *in vitro* and *in vivo*, suggesting that both cell lines tested are suitable for the assessment of NM toxicity. In summary, the results presented here highlight the need to carefully review model systems to decipher the extent to which they can replace *in vivo* assays.



## 1. Introduction

The high variability of physicochemical properties of nanomaterials (NMs) renders them valuable for a wide range of applications, *e.g.* cosmetics, textiles, packaging, electronics, and medical devices (Stark et al., 2015). Moreover, new NM variants are continuously being developed and previous studies have shown that especially silica or titanium dioxide NMs are among those with the highest production volumes of 5500–2400,000 t and 3000–88,000 t worldwide per year, respectively (Commission, 2012; Holden et al., 2014; Keller et al., 2013; Piccinno et al., 2012). This makes a detailed characterization of their potential health effects indispensable.

So far, regulatory risk assessment mainly depends on *in vivo* testing, even though animal tests are time-consuming, costly, and ethically questionable. However, replacing animal tests with *in vitro* assays is challenging. Up to now, much afford has been undertaken to develop integrated approaches to testing and assessment (IATAs) combining several *in chemico, in vitro*, and *in vivo* tests in a structured manner, employing specific decision trees (OECD, 2018). The development of IATAs is strongly connected to the development of Adverse Outcome Pathways (AOPs) (OECD, 2012), and insights into the modes of action (MoAs) are of utmost importance for the latter. Omics approaches can provide extensive information about cellular responses to NMs. Among the various omics techniques, in praxis, transcriptomics reveals the most comprehensive information, but proteomics and metabolomics are closer to the phenotype (Costa and Fadeel, 2016; Steuer et al., 2019; Wishart, 2016). The shortcomings of single omics techniques can be overcome by integrating multiple omics into one mechanism-oriented analysis, and we have previously shown that using several omics approaches facilitates unraveling NMs MoAs (Bannuscher et al., 2019; Karkossa et al., 2019), helps to develop NM grouping strategies, and to identify relevant physicochemical properties (Bannuscher et al., 2019; Karkossa et al., 2019). Here, we focused on NMs MoAs *in vitro* and *in vivo* and on the transferability of both approaches.

Since the lung is considered the main entry portal for airborne NMs (Bakand et al., 2005), we investigated effects on the lung *in vitro* and *in vivo*. If NMs reach the alveoli, they can be cleared by macrophages, which can phagocytose NMs (Geiser, 2002). Inside the alveoli, epithelial cells form a barrier between gas phase and blood circulation (Fröhlich and Salar-Behzadi, 2014; Muhlfeld et al., 2008) and can take up NMs (Kreyling et al., 2002; Oberdörster et al., 2005; Semmler-Behnke et al., 2007; Semmler et al., 2004). By transcytosis through the epithelial cells, NMs may travel into the interstitial space, from where they can enter the lymph nodes and the blood circulation, thus leading to potential adverse effects in secondary organs (Geiser and Kreyling, 2010; Kreyling et al., 2010; Kreyling et al., 2013; Stone et al., 2017). Hence, alveolar macrophages and alveolar epithelial cells are relevant model systems to investigate NM effects *in vitro*, and well-established rat cell lines of alveolar macrophages (NR8383) and alveolar epithelial type II cells (RLE-6TN) were used in the present study to analyze the effects of four silica-based NMs (SiO2_15_Amino, SiO2_15_Unmod, SiO2_7 and SiO2_40) as well as one titanium dioxide-based NM (TiO2_NM105). While SiO2_15_Amino and SiO2_15_Unmod are precipitated NMs, SiO2_40 and SiO2_7 are pyrogenic (fumed).

Furthermore, the effects that were observed *in vitro* were compared to those *in vivo* to investigate the applicability of these *in vitro* model systems for NM risk assessment. For this purpose, short-term inhalation studies (STIS) and intratracheal instillation studies with rats were performed, since both were shown to be suitable to classify NMs (Landsiedel et al., 2014; Morimoto et al., 2016). Due to short follow-up periods, both methods focus on the detection of early adverse effects, such as inflammation or beginning histological changes. Importantly, both methods have advantages and disadvantages. While STIS reflect the physiological way of NMs entering the lung as an aerosol, instillations are easier to handle, and the actual dose delivered to the lung is highly reliable. Also, an administration of particles *via* instillation requires a vehicle, in which the NMs need to be suspended. This vehicle may alter the physicochemical properties of the NMs and influence their distribution in the lung (Driscoll et al., 2000). However, the instillation approach provides particles at a high dose rate, which is more similar to most *in vitro* approaches. Therefore, both techniques were applied in the present study, followed by proteomics and metabolomics analyses on lung samples of the rats.

One of the most important biological effects of NMs is reported to be the formation of reactive oxygen species (ROS), which may result in inflammation and thus possibly adverse effects (Fubini and Hubbard, 2003). The formation of ROS and the emergence of adverse effects depend on the physicochemical properties of the used NMs, although the detailed mechanisms are not fully understood (Fubini and Hubbard, 2003; Huang et al., 2010). In particular, metal oxide-based NMs can induce ROS formation through the release of transition metals. Furthermore, the presence of pro-oxidative functional groups or the binding of environmental contaminants to the NM surface can support the production of ROS and thus influence their toxicity (Risom et al., 2005). Under normal conditions, these ROS can be neutralized by antioxidants, but when ROS levels increase beyond the neutralization capacity, oxidative stress emerges (Sies). To describe the different levels of oxidative stress, a stratified oxidative stress model has been developed (Li et al., 2002; Li et al., 2008; Nel et al., 2006; Xiao et al., 2003). This tiered model describes the dependence of the oxidative stress level on the ratio of reduced glutathione (GSH) to oxidized glutathione (GSSG). GSH is an antioxidant, which is oxidized to GSSG during its neutralization of ROS. Under normal conditions, the GSH/GSSG ratio is high. However, it decreases when there is a disproportionate increase in ROS, a process whose biological consequences can be described by three tiers: In tier 1, the expression of antioxidants is induced by nuclear factor erythroid 2-related factor 2 (Nrf2), followed by inflammatory responses mediated by nuclear factor kappa-light-chain-enhancer of activated B cells (Nfκb) and activator protein 1 (Ap-1) in tier 2, and cytotoxicity in tier 3 (Huang et al., 2010; Li et al., 2008; Nel et al., 2006). Since the level of oxidative stress has a major impact on the development of adverse effects upon NM treatment (Manke et al., 2013; Mendoza and Brown, 2019), we aimed to perform a detailed analysis of the levels of oxidative stress using integrative omics analysis. In addition, we compared *in vitro* and *in vivo* results to compare the effects on a mechanistic level and to clarify the extent to which animal tests could be replaced by cellular experiments in future risk assessment.

## 2. Methods

### 2.1. Study design

With the present study, we investigated the effects of four silica-based NMs (SiO2_15_Amino, SiO2_15_Unmod, SiO2_7, SiO2_40) and TiO2_NM105 as benchmark material *in vitro* and *in vivo* applying untargeted proteomics and targeted metabolomics.

The applied study design is depicted in Additional file 2 (Fig. S1) to point out the experimental setup (model systems, NMs studied, doses applied, exposure times) and previous publications of the data obtained.

As the main aim of this study was to gain mechanistic insights, we mainly investigated NMs that have been extensively characterized previously (SiO2_15_Amino, SiO2_15_Unmod, TiO2_NM105), *e.g. in vitro* with alveolar macrophages to determine toxicological endpoints (Wiemann et al., 2016) and *in vivo* with STIS revealing information on bronchoalveolar lavage fluids (BALFs), histological, and pathological changes (Landsiedel et al., 2014). However, to our knowledge, dose- and time-dependent mechanistic insights focusing on alveolar toxicity and applying proteomics and metabolomics have not been obtained for any of these otherwise well-characterized NMs. Thus, we considered these five NMs to be well suited for comparison of mechanistic effects on alveolar type II cells and alveolar macrophages as well as on rat lungs after *in vivo* exposure, either by STIS or by instillation.

In brief, NM effects were investigated *in vitro* using rat alveolar type II cells (cell line RLE-6TN) and rat alveolar macrophages (cell line NR8383). Proteins and metabolites were obtained from individual samples. To gain insights into NM effects *in vivo*, short-term inhalation studies (STIS) and instillations were performed with rats. STIS were performed with doses up to 50 mg/m$^3$, corresponding to 11.9–23.8 μg/cm$^2$ *in vitro,* assuming deposition of about 5–10% (Haase et al., 2017). Accordingly, *in vitro* studies were conducted at 0.1–50 μg/cm$^2$, depending on the cytotoxicity of the NMs tested in the two cell lines, which has been previously described for alveolar type II cells (Karkossa et al., 2019) as well as alveolar macrophages (Bannuscher et al., 2019) and was summarized in Additional file 2 (Tables S1 and S2, respectively). Instillations were performed with 0.09–0.36 mg NM, corresponding to 0.064–0.016 μg/cm$^2$, assuming that the full dose was deposited on an average rat lung surface area of 5571 cm$^2$ (Johanson and Pierce, 1973). For STIS and instillations, proteins and metabolites were extracted from the lungs of the same animals.

### 2.2. Selected NMs and NM dispersion

SiO2_15_Amino and SiO2_15_Unmod (both precipitated) were provided in suspension by BASF SE. SiO2_7 and SiO2_40 (both pyrogenic) were manufactured by Evonik Industries and provided as powder. TiO2_NM105 was obtained as a powder from the JRC repository. The physicochemical properties for these NMs have been described in detail earlier (Bannuscher et al., 2019; Karkossa et al., 2019). A summary of selected properties can be found in Table 1. Before use, the NMs were dispersed by an indirect probe sonication protocol (Taurozzi et al., 2011) as described before (Bannuscher et al., 2019; Karkossa et al., 2019) and specified in Additional file 2.

**Table 1**
Summary of key physicochemical properties of the investigated NMs.
Shown are the core materials, the primary particle sizes (PPS) as given by the manufacturer, the surface areas as determined by BET, and the agglomerate sizes determined by dynamic light scattering (DLS). The physicochemical properties of these NMs were described before in detail (Bannuscher et al., 2019; Driessen et al., 2015; Karkossa et al., 2019; Landsiedel et al., 2014; Wiemann et al., 2016; Wiemann et al., 2018).

| Name | Core material | PPS | Surface area (BET) | Agglomerate size in F12K with serum (DLS) | Agglomerate size in water (DLS) |
|---|---|---|---|---|---|
| | | [nm] | [m$^2$/g] | [nm] | [nm] |
| SiO2_15_Unmod | Silica | 15 | 200 | 42.2 | 48.3 |
| SiO2_15_Amino | | 15 | 200 | 144.2 | 47.5 |
| SiO2_40 | | 40 | 50 | 255.0 | 373.4 |
| SiO2_7 | | 8 | 300 | 275.1 | 243.3 |
| TiO2_NM105 | Titanium dioxide | 21 | 51 | 3490.0 | 394.1 |

### 2.3. Cell culture

Cell culture of alveolar macrophages (cell line NR8383, ATCC, CRL-2192, USA) (Bannuscher et al., 2019; Wiemann et al., 2016) and alveolar type II cells (cell line RLE-6TN, ATCC, CRL-2300, USA) (Karkossa et al., 2019) was conducted as described before for optimal comparability with previous studies. Details can be found in Additional file 2.

Macrophages were exposed to 11.25, 22.5, and 45 μg/ml of SiO2_15_Amino, SiO2_15_Unmod, SiO2_40, SiO2_7, or TiO2_NM105 for 24 h under serum-free conditions. Thus, assuming complete sedimentation, the nominal doses were 2.5, 5, and 10 μg/cm$^2$. The results obtained with this experimental setup have already been described for some selected proteins and metabolites (Bannuscher et al., 2019) (Additional file 2: Fig. S1).

Type II cells were treated with 1, 10, or 50 μg/cm$^2$ silica NMs. Only TiO2_NM105 was investigated at doses of 0.1, 1, and 10 μg/cm$^2$ due to its high cytotoxicity. The results of TiO2_NM105 after 24 h were briefly described in one of our previous studies (Karkossa et al., 2019) (Additional file 2: Fig. S1). To compare the results in type II cells with those in macrophages, a 24 h exposure was examined with targeted metabolomics and untargeted proteomics of type II cells as well. Additionally, targeted metabolomics were performed after 48 h of exposure and untargeted proteomics after 6 h and 48 h of exposure of type II cells.

For macrophages, three to four replicates were used for metabolomics and four replicates for proteomics. For type II cells, the metabolomics approach was conducted in four replicates, whereas proteomics was performed in four to five replicates.

### 2.4. Short-term inhalation studies (STIS)

STIS were conducted with SiO2_7 and TiO2_NM105 under the agreement «UN 18 306 DO» approved by the Committee on the Ethics of Animal Experiments of the University of Namur. The procedure has been described before (Bannuscher et al., 2020). Briefly, non-pregnant female Wistar rats (Charles River, France), aged 7–8 weeks and weighing 180–200 g at the beginning of the experiments, were exposed (using whole-body exposure) to the nanoaerosols for 6 h/d over 5 consecutive days or to filtered air (controls) and either sacrificed immediately after exposure (exposure groups, E) or 21 d after exposure (recovery groups, R) by intraperitoneal Nembutal injection of 60 mg/kg (Ceva Sante Animale, France) after anesthesia. Five rats were used for each group. Lungs were frozen directly in liquid nitrogen and used for proteomics and metabolomics. Since more effects for SiO2_7 than TiO2_NM105 were observed in the *in vitro* studies, STIS were performed with 0.5, 2, and 5 mg/m$^3$ SiO2_7 in both exposure and recovery groups. TiO2_NM105 was studied at doses of 0.5, 2, and 10 mg/m$^3$ in both exposure and recovery groups, resulting in only few significant changes. Hence, 50 mg/m$^3$ TiO2_NM105 was additionally tested in the exposure group.

### 2.5. Instillation studies

The experimental design for intratracheal instillation with SiO2_15_Amino, SiO2_15_Unmod, SiO2_7, and SiO2_40 was approved by The Ethics Committee of the "Vasile Goldis" Western University of Arad and authorized by the National Sanitary Veterinary and Food Safety Authority of Romania with registration no. 007/27.11.2017. The procedure used has been described previously (Bannuscher et al., 2020). In brief, male Wistar rats from the "Cantacuzino" National Institute of Research (Bucharest, Romania) were used. For instillation, the rats were anesthetized by intraperitoneal injection of a ketamine/xylazine cocktail (100/10 mg/kg body weight) and subsequently exposed to 0.36, 0.18, or 0.09 mg NM in 50 μl PBS. Either rats were euthanized under anesthesia 3 d after this single exposure (exposure groups, E) or after an additional recovery time of 21 d (recovery group, R). Four

rats were used for each group. Lungs were frozen directly in liquid nitrogen and used for proteomics and metabolomics.

### 2.6. Sample preparation for omics studies

For *in vitro* samples, preparation was performed as described before (Bannuscher et al., 2019; Karkossa et al., 2019). Metabolites and proteins were extracted from individual samples. In brief, to isolate proteins, RIPA buffer containing 0.05 M Tris/HCl (pH 7.4, Roth, Germany), 0.15 M NaCl (Roth, Germany), 0.001 M EDTA (Roth, Germany), 1% Igepal (Sigma Aldrich, Germany), 0.25% Na-deoxycholate (Sigma Aldrich, Germany), 10 mM Na-Pyrophosphate (Sigma Aldrich, Germany), 10 mM β-Glycerolphosphate (Sigma Aldrich, Germany), 1 mM Sodiumorthovanadate (Sigma Aldrich, Germany), 10 μl/ml Protease-inhibitor (Merck Millipore, USA), 10 μl/ml β-Mercaptoethanol, 10 μl/ml NaF, and 2 μl/ml Na was added to the washed cells. Next, samples were shaken (10 min, 4 °C), cell debris was collected, samples were frozen at −80 °C, thawed, rotated (30 min, 4 °C), and centrifuged (30 min, 12,000*g*, 4 °C). Protein concentration was determined using the Bradford assay (Bio-Rad, USA). In contrast, metabolites were extracted by addition of 5% chloroform, 45% methanol, and 50% water followed by rotation (30 min, 4 °C) and centrifugation (10 min, 500*g*, 4 °C).

After STIS and instillations, frozen lungs were homogenized as previously described (Bannuscher et al., 2020), and proteins as well as metabolites were extracted from the lungs of the same rats according to the *in vitro* studies.

### 2.7. Targeted metabolomics and untargeted proteomics

The metabolomics data presented here have been previously published (Bannuscher et al., 2020) but were reanalyzed for this comparison study in analogy to the proteomics data (Additional file 2: Fig. S1) to assure comparability of proteomics and metabolomics results.

In brief, the AbsoluteIDQ p180 Kit (Biocrates, Austria) was used as previously described (Bannuscher et al., 2020; Bannuscher et al., 2019; Karkossa et al., 2019; Potratz et al., 2017), and samples were analyzed using an API 5500 triple quadrupole mass spectrometer (ABSciex, Germany) coupled to an Agilent 1260 Infinity HPLC system (Agilent, USA). Analyst® software and MetIDQ were used for data analysis. Subsequent analysis was performed as described before (Bannuscher et al., 2019; Karkossa et al., 2019), normalizing the resulting metabolite concentrations to the respective cell numbers and excluding values below the detection limit. Fold changes (FCs, treatment *vs.* control) of the average values were log2-transformed and used for further analyses.

For untargeted proteomics, tandem mass tag (TMT) labeling (Thermo Scientific, USA) was applied. Therefore, 25 μg protein per sample was used, and labeling was conducted with 0.1 mg label.

For type II cells, the workflow was performed according to the manufacturer's instructions and as previously described (Karkossa et al., 2019; Thompson et al., 2003; Wewering et al., 2016). For these samples, TMT-6-plex (Thermo Scientific, USA) was used, while for all other sample sets TMT-10-plex (Thermo Scientific, USA) labeling was applied.

Effects on macrophages were investigated as previously described (Bannuscher et al., 2019). In brief, paramagnetic beads were used, resulting in improved sample quality and allowing fractionation (Hughes et al., 2014; Hughes et al., 2019; Wang et al., 2021). The paramagnetic bead approach was also applied to the protein samples from the *in vivo* studies.

As described before (Bannuscher et al., 2019; Karkossa et al., 2019), labeled samples were analyzed on a nano-UPLC system (Ultimate 3000, Dionex, USA) with trapping column (Acclaim PepMap 100 C18, 3 μm, nanoViper, 75 μm × 5 cm, Thermo Fisher, Germany) and analytical column (Acclaim PepMap 100 C18, 3 μm, nanoViper, 75 μm × 25 cm, Thermo Fisher, Germany). A non-linear gradient of 150 min was applied for peptide separation. The eluting peptides were ionized using a chip-based ESI source (Nanomate, Advion, USA) coupled to the mass spectrometer (QExactive HF, Thermo Scientific, USA). MS raw data were processed using ProteomeDiscoverer 2.2. The database search was performed against the UniprotKB reference proteome of *Rattus norvegicus* (27 February 2019), resulting in replicate FCs (treatment *versus* control), which were log2-transformed and median-normalized before further analyses.

### 2.8. Statistical analysis

Statistical analysis of log2-transformed FCs of proteins and metabolites was performed in R-3.5.0 using multiple packages (Graffelman, 2019; Gu et al., 2014; Mahto, 2018; Neuwirth, 2014; Spiess, 2018; Warnes et al., 2016; Wickham, 2011; Wickham, 2016; Wickham and Bryan, 2018; Wickham and Henry, 2018). To detect significant changes compared to controls, Student's *t*-test with Benjamini & Hochberg adjustment was performed for proteins and metabolites that were quantified in at least three biological replicates. FCs and adjusted *p*-values (p.adj) for all data sets can be found in Additional file 1 (Tables E3–E10) along with replicate values and calculation results (Tables E11–E24).

Enrichment analyses were performed using Ingenuity Pathway Analysis (IPA, Qiagen, Germany) (Krämer et al., 2013; Qiagen). For this purpose, the data were filtered for significantly (p.adj ≤ 0.05) altered proteins and metabolites, lung was selected as tissue and rat as organism. The mapping of metabolites to identifiers from the Human Metabolome Database (HMDB) used for this analysis can be found in Additional file 1 (Table E2), where the mapping of Uniprot Accessions to genes is also stored (Table E1). Furthermore, the obtained IPA results are summarized in Additional file 1 (Tables E25–E30) for all data sets.

## 3. Results

To gain insights into NMs MoAs, the effects of four silica NMs (SiO2_15_Unmod, SiO2_15_Amino, SiO2_40, SiO2_7) and TiO2_NM105 were investigated *in vitro* and *in vivo*. In this context, some of the selected NMs (SiO2_15_Unmod, SiO2_15_Amino, TiO2_NM105) have already been extensively characterized, determining, for example, toxicological endpoints in alveolar macrophages (Wiemann et al., 2016) and BALFs, histological, and pathological changes after STIS (Landsiedel et al., 2014). The physicochemical properties of these NMs have been described previously (Bannuscher et al., 2019; Driessen et al., 2015; Karkossa et al., 2019; Landsiedel et al., 2014; Wiemann et al., 2016; Wiemann et al., 2018), and a summary of the main physicochemical properties is provided in Table 1.

### 3.1. In vitro investigations

First, the effects of these five NMs were investigated *in vitro* in alveolar type II cells and alveolar macrophages at three different doses after an exposure time of 24 h.

#### 3.1.1. SiO2_40, SiO2_7, and TiO2_NM105 induce most significant changes in vitro

Changes in protein (Additional file 2: Figs. S2–S5) and metabolite (Additional file 2: Figs. S6–S9) abundances were considered relative to untreated controls, and the summary of percentages of significantly (p.adj ≤ 0.05) altered proteins and metabolites (Fig. 1a) shows that significant changes for metabolites occurred only at the highest dose investigated (10 μg/cm$^2$ for TiO2_NM105 and 50 μg/cm$^2$ for the other NMs tested) in type II cells. Interestingly, the pyrogenic NMs SiO2_40 and SiO2_7 as well as TiO2_NM105 were the only NMs that had significant effects on metabolites even at a dose of 10 μg/cm$^2$ in type II cells and macrophages, at which none of the other tested NMs resulted in significant alterations (Additional file 2: Figs. S6–S9). TiO2_NM105 showed significantly changed metabolites at a dose of 10 μg/cm$^2$ in type II cells but not in macrophages. In contrast, almost no significantly

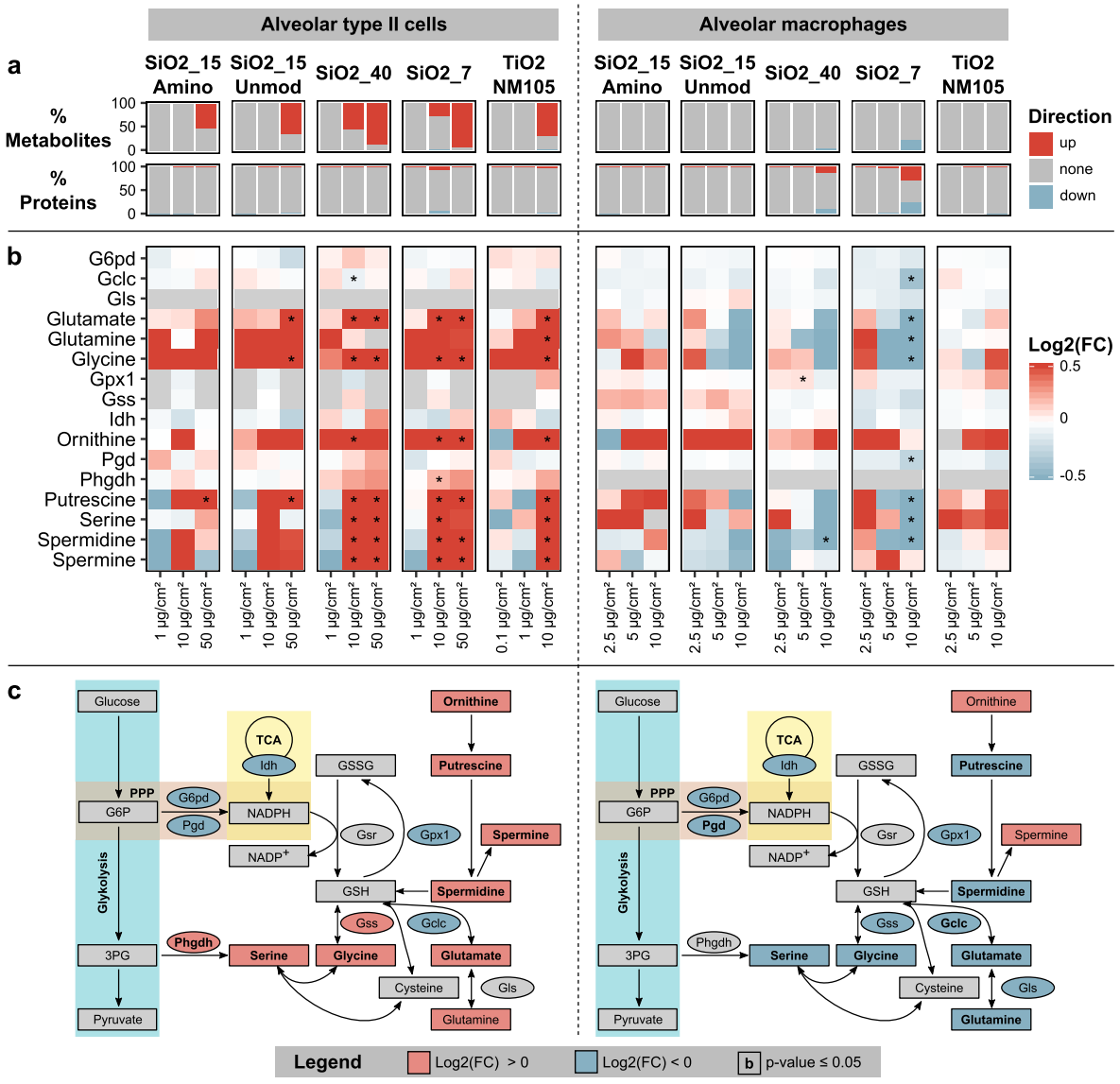


**Fig. 1.** Summary of *in vitro* results focusing on the GSH/GSSG pathway.
The percentages of significantly altered (p.adj ≤ 0.05) metabolites and proteins after exposure of type II cells (left) and macrophages (right) are shown for the five different NMs administered at different doses (a). The observed changes were summarized for proteins and metabolites associated with the GSH/GSSG pathway (Cohen and Hochstein, 1963; Dickinson and Forman, 2002; Kanehisa, 2019; Kanehisa and Goto, 2000; Kanehisa et al., 2019; Meister and Anderson, 1983; Richman and Meister, 1975), and significant changes are indicated with an asterisk (b). Furthermore, the effects observed for the GSH/GSSG pathway after treatment with 10 μg/cm$^2$ SiO2_7 are presented for the two cell lines, where significant changes are indicated with bold letters (c).

altered proteins were observed in type II cells, whereas dose-dependent increases in the percentage of significantly altered proteins were noticed for SiO2_40 and SiO2_7 after macrophage treatment. In agreement with our previous studies, SiO2_40, SiO2_7, and TiO2_NM105 were therefore considered "active" NMs (Bannuscher et al., 2019; Karkossa et al., 2019), while SiO2_15_Unmod and SiO2_15_Amino were classified as "passive".

Additionally, exposure times of 6 h and 48 h were examined for type II cells using proteomics. After 6 h of NM treatment, a maximum of 72 significantly altered proteins were observed for 10 μg/cm$^2$ SiO2_7 compared with 220 and 462 proteins under the same conditions but after 24 h and 48 h of incubation, respectively (Additional file 1: Table E3). Thus, the 6 h time point was excluded from further analyses.

For the significantly (p.adj ≤ 0.05) altered proteins and metabolites, enrichment analysis was performed, which showed mainly enrichment of signaling pathways associated with oxidative stress, *e.g.* mitochondrial dysfunction, Nrf2-mediated oxidative stress response, and oxidative phosphorylation (Additional file 2: Fig. S10). Therefore, we next focused on examining the extent of oxidative stress achieved under the conditions tested. For this purpose, we used only the results after 24 h of treatment, since only small time-dependent changes were observed between 24 h and 48 h in type II cells (Additional file 2: Figs. S10 and S11).

### *3.1.2. In vitro exposure oppositely affects proteins and metabolites involved in GSH/GSSG signaling in type II cells and macrophages*

Since the GSH content is highly related to the generation of oxidative stress, proteins and metabolites associated with GSH/GSSG signaling (Cohen and Hochstein, 1963; Dickinson and Forman, 2002; Kanehisa, 2019; Kanehisa and Goto, 2000; Kanehisa et al., 2019; Meister and Anderson, 1983; Richman and Meister, 1975) were first examined (Fig. 1b).

In type II cells (Fig. 1b, left), SiO2_40, SiO2_7, and TiO2_NM105 were the only NMs that elicited significant changes after treatment with 10 μg/cm$^2$, which is the dose we used in previous screening experiments with twelve NMs in type II cells (Karkossa et al., 2019).

Interestingly, SiO2_15_Unmod and SiO2_15_Amino showed the same trends, with SiO2_15_Unmod leading to higher increases (expressed as Log2(fold changes), Log2(FCs)) than SiO2_15_Amino. Overall, the NM treatment of type II cells resulted in increased abundances of proteins and metabolites that are part of the GSH/GSSG signaling, indicating an increased GSH production, especially in the case of SiO2_40, SiO2_7, and TiO2_NM105, confirming that not only SiO2_40 and SiO2_7 are "active" NMs, but also TiO2_NM105, which is consistent with our previous study (Karkossa et al., 2019).

Interestingly, the opposite effects were observed in macrophages (Fig. 1b, right) compared to type II cells (Fig. 1b, left). In macrophages, the most significant changes were obtained for SiO2_7 and SiO2_40 at the highest dose studied, 10 μg/cm$^2$. SiO2_15_Unmod showed the same trends, although with less significance. The decreased abundances of proteins and metabolites suggest reduced GSH production for these three NMs in macrophages. This, in turn, may have resulted in inadequate neutralization of the ROS that appeared, triggering further oxidative stress responses. The opposite changes in type II cells and macrophages occurred mainly upon treatment with 10 μg/cm$^2$ SiO2_7 (Fig. 1c).

*3.1.3. Oxidative stress levels induced in type II cells and macrophages are different*

To clarify whether the observed effects on GSH/GSSG signaling in the two cell lines led to a different assignment to the three tiers of oxidative stress, the changes in proteins and metabolites associated with these tiers were investigated. Specifically, induction of tier 1 is accompanied by the activation of Nrf2 targets, tier 2 by Nfκb and Ap-1 targets, and tier 3 by cytotoxicity (Huang et al., 2010; Li et al., 2008; Nel et al., 2006).

*3.1.3.1. Proteins associated with tier 1.* Notably, all proteins identified in the present study relevant to the maintenance of GSH/GSSG homeostasis (Fig. 1b, c) are regulated by the transcription factor Nrf2 (DeNicola et al., 2015; Hayes and Dinkova-Kostova, 2014; Jung and Kwak, 2010; Morales Pantoja et al., 2016), the hallmark of tier 1. Thus, at the highest applied dose of 10 μg/cm$^2$ for TiO2_NM105 and 50 μg/cm$^2$ for the other NMs, the NMs likely resulted in tier 1 in type II cells. In macrophages, decreased abundances of analytes associated with GSH/GSSG signaling were observed for SiO2_7, SiO2_40, and SiO2_15_Unmod, suggesting that these three NMs led to a decreased GSH/GSSG ratio, whereas SiO2_15_Amino and TiO2_NM105 did not.

In addition to proteins that are part of GSH/GSSG signaling, Gstm1, Nqo1, Hmox1, Txn, Txnrd1, Cat, Sod1, Sod2, and Lamp2 have been described as Nrf2 targets (Hayes and Dinkova-Kostova, 2014; Jung and Kwak, 2010; Pajares et al., 2018) and thus appear to be relevant to tier 1.

*3.1.3.2. Proteins associated with tier 2.* To investigate whether tier 2 was also induced, the data were screened for Nfκb and Ap-1 targets and hence for inflammatory processes. Importantly, several of the previously described Nrf2 targets also have a binding position for Nfκb or Ap-1. Examples include Gclc, Idh, Pgd, Phgdh, Hmox1, Nqo1, Cat, Sod2, and Lamp2 (Sawada et al., 1993; Yang et al., 2016). In addition, Icam1 (Lee and Yang, 2013; Rahman and MacNee, 1998), Il18 (Grandjean-Laquerriere et al., 2007; Li et al., 2016), B2m (Gobin et al., 2003), Tnfaip8 (Niture et al., 2018), and Bax (Huang et al., 2007; Kim et al., 2010) have been described as targets of Nfκb or Ap-1 and related to either inflammation or apoptosis. Another candidate is Ccr1, which is expressed mitogen-activated protein kinase (Mapk)-dependently (Ko et al., 2007). Since chemokine/chemokine receptor interactions are relevant for immune cell migration, Ccr1 is an important candidate to investigate whether tier 2 has been induced. Furthermore, the absence of Ccr1 in mice has been shown to result in diminished inflammatory responses and increased mortality (Domachowske et al., 2000).

*3.1.3.3. Proteins and metabolites associated with tier 3.* Finally, candidates reflecting tier 3 and thus cytotoxicity were examined. Besides Bax (Brunelle and Letai, 2009), which was assigned to tier 2 in the present study because it is an Nfκb target protein (Huang et al., 2007; Kim et al., 2010), Vdac1 is involved in mitochondrial pore formation and thus in the induction of apoptosis (Madesh and Hajnóczky, 2001) and consequently should be assigned to tier 3. Furthermore, it has been shown that increased citric acid cycle (TCA) leads to increased formation of ROS, followed by apoptosis (Brookes et al., 2004). In addition to the proteins already mentioned, Glud1 and Fh are involved in TCA (Akram, 2014; Krebs, 1970) and were therefore assigned to tier 3. Also, sphingomyelins (SMs), which belong to the sphingolipid class and are mainly found in plasma membranes and lipoproteins, are relevant for the formation of ROS. SMs are hydrolyzed in response to oxidative stress, leading to the formation of ceramides, which are second messengers involved in the induction of apoptosis. However, the specific mechanisms are not yet fully understood (Andrieu-Abadie et al., 2001; Andrieu-Abadie and Levade, 2002).

*3.1.3.4. Mainly tier 1 is affected in type II cells, while all tiers are affected in macrophages.* A summary of all the analytes mentioned and their assignment to the different tiers of oxidative stress can be found in Additional file 2 (Tables S3 and S4). In type II cells, almost no significant changes were noticed for all these candidates up to the highest tested dose of 50 μg/cm$^2$ (Fig. 2a), whereas treatment of macrophages with 10 μg/cm$^2$ SiO2_40 and SiO2_7 led to significant changes. Importantly, SiO2_15_Unmod again showed the same trends as SiO2_40 and SiO2_7, but the effects were less pronounced. Furthermore, large differences were again evident between type II cells and macrophages, particularly after treatment with 10 μg/cm$^2$ SiO2_7 (Fig. 2b).

For type II cells, significant changes appeared only in proteins that are Nrf2 target genes, confirming that only tier 1 of oxidative stress was affected in type II cells under the tested conditions. The significantly affected proteins were Sod1, Txn, Gstm1, and Lamp2. In contrast, the macrophages resulted in significant changes in all tiers after treatment with 10 μg/cm$^2$ SiO2_7. Interestingly, there are several cases where opposite changes in protein abundance were visible in type II cells and macrophages. Examples are Sod1 and Sod2 with opposite changes in each other and additionally opposite changes in the two cell lines studied. The fact that Sod1 and Sod2 resulted in different directions of change can be explained by their localization within the cell. While Sod1 is found in the cytoplasm, Sod2 is responsible for neutralizing ROS in the mitochondria. Moreover, both proteins possess not only an Nrf2-binding site but also an Nfκb-binding site in their promoter region. Whereas the Nfκb binding site in Sod1 has been described as relatively insensitive, the binding site in Sod2 appears to be very sensitive (Miao and St Clair, 2009), suggesting that Sod1 expression is primarily induced by Nrf2, while Sod2 expression may be induced by Nfκb. This is additional evidence that type II cells led only to tier 1, whereas in macrophages all three tiers were initiated.

*3.2. In vivo investigations*

Next, we investigated the *in vivo* effects of SiO2_7 and TiO2_NM105 with STIS and of SiO2_15_Amino, SiO2_15_Unmod, SiO2_7, and SiO2_40 by instillation. For both methods, changes in the lung proteome and metabolome were examined at different doses. Exposure groups (E) were sacrificed directly after treatment of 5 d or 3 d for STIS and instillations, respectively. In contrast, the recovery groups (R) had a recovery period of 21 d after the treatment period.

*3.2.1. SiO2_7 and TiO2_NM105 induced significant changes upon STIS*

The percentages of significantly altered proteins (Additional file 2: Figs. S12–S13) and metabolites (Additional file 2: Figs. S16–S17) showed dose-dependent increases of significantly altered analytes mainly for the STIS exposure groups (Fig. 3a). Among them, the most significant changes occurred at 50 mg/m$^3$ TiO2_NM105 in the STIS exposure group. Importantly, this dose was used only for the

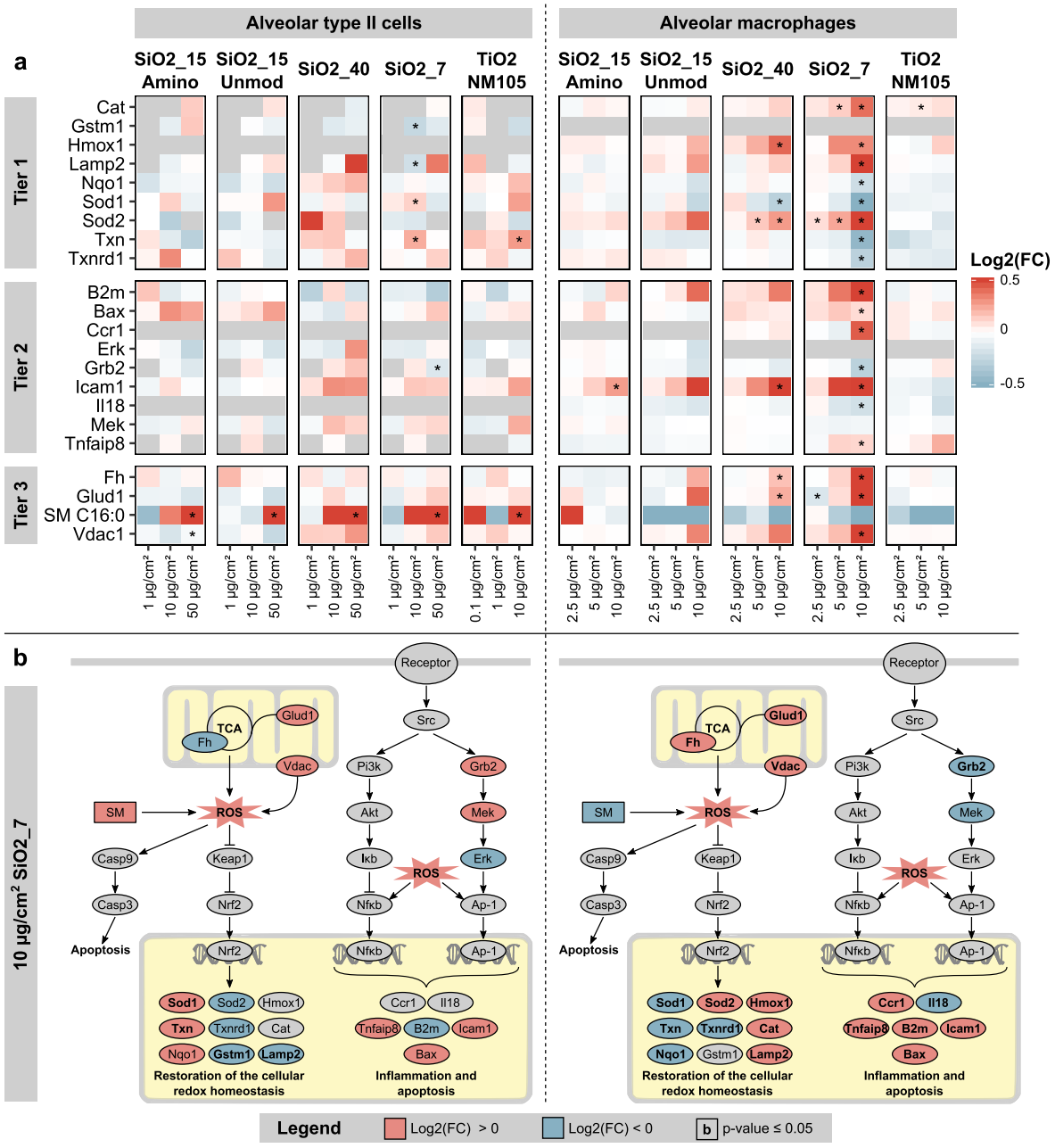


**Fig. 2.** Summary of *in vitro* results focusing on the tiers of oxidative stress.
Shown are the changes after treatment of type II cells (left) and macrophages (right) with different NMs at different doses for analytes associated with the tiers of oxidative stress. In tier 1, expression of Nrf2 targets is induced, tier 2 is accompanied by Nfκb and Ap-1 targets and thus inflammatory processes, and tier 3 by cytotoxicity (Huang et al., 2010; Li et al., 2008; Nel et al., 2006). Significant changes (p.adj ≤ 0.05) are indicated with an asterisk (a). Furthermore, the effects observed for the three tiers after treatment with 10 µg/cm² SiO2_7 are presented for the two cell lines, where significant changes are indicated with bold letters (b).

TiO2_NM105 exposure group, whereas TiO2_NM105 was tested only up to a dose of 10 mg/m³ in the recovery groups. Besides, the effects of SiO2_7 were assessed only up to a dose of 5 mg/m³ in exposure and recovery groups, as it showed a considerable number of significant changes already at this dose.

### *3.2.2. SiO2_15_Amino, SiO2_15_Unmod, SiO2_7, and SiO2_40 induced significant changes upon instillation*

Instillations were performed up to a dose of 0.36 mg in exposure and recovery groups for all four NMs studied and significantly altered (p.adj ≤ 0.05) proteins (Additional file 2: Figs. 14-15) and metabolites (Additional file 2: Figs. 18-19) were determined relative to untreated controls. The results (Fig. 3a) show that SiO2_7 and SiO2_40 did not induce significantly altered metabolites under any of the conditions. In contrast, a high number of significantly altered metabolites was detected for the putatively less "active" NMs SiO2_15_Amino and SiO2_15_Unmod. Since the increased numbers of significantly altered proteins for SiO2_7 and SiO2_40 compared with the other two NMs indicate stronger effects for SiO2_7 and SiO2_40, the lack of changes in the metabolome could be explained by overwhelming effects that were no longer reproducibly detectable.

### *3.2.3. No clear assignment to oxidative stress levels is possible for STIS and instillation results*

It is noteworthy that the assignment to the three tiers of oxidative stress was not as clear *in vivo* (Fig. 3b) as in the *in vitro* results, although

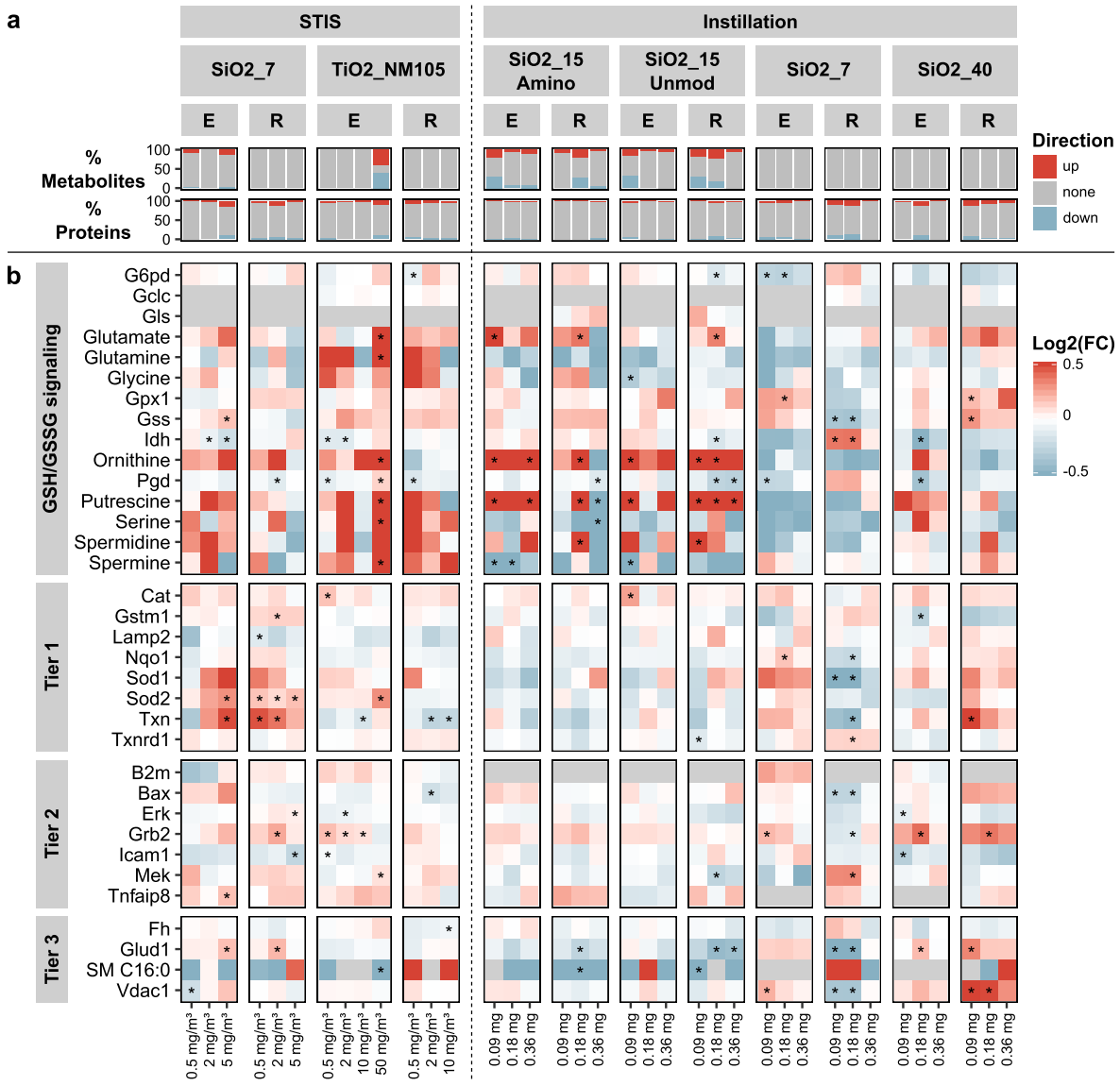


**Fig. 3.** Summary of *in vivo* results focusing on the tiers of oxidative stress.
Shown are the percentages of significantly altered (p.adj ≤ 0.05) metabolites and proteins after STIS (left) and instillations (right) for the five different NMs administered at different doses, distinguishing between exposure groups (E) and recovery groups (R) (a). Furthermore, the observed changes for proteins and metabolites associated with the GSH/GSSG pathway and the tiers of oxidative stress are summarized and significant changes are indicated with an asterisk (b).

significant changes were observed for all three tiers, especially in the case of SiO2_7, SiO2_40, and TiO2_NM105, suggesting that they are "active" *in vivo*. In addition, analytes with dose-dependent changes, *e.g.* Ornithine, Sod1, Sod2, and Txn, were detectable mainly for the STIS exposure group of SiO2_7.

The different results of assignment to the three tiers *in vitro* and *in vivo* can be explained by the cellular composition of rat lungs (Fig. 4a), with only 14.2% alveolar type II epithelial cells and 3% alveolar macrophages (Crapo et al., 1982), and the fact that the two cell types examined here showed opposite effects. Comparison of Log2 (FC) distributions of analytes associated with the three tiers of oxidative stress after treatment with SiO2_7 *in vitro* and *in vivo* (Fig. 4b) exemplifies this. For GSH/GSSG signaling, opposite effects were obtained for type II cells and macrophages, but no clear trends were observed in STIS and instillations. There were also no clear trends for analytes associated with the three tiers. However, the higher distribution ranges (Fig. 4b) revealed increased changes in macrophages and STIS, suggesting that these model systems are more sensitive.

### *3.2.4. STIS and instillations showed altered inflammatory responses rather than altered oxidative stress responses*

Since GSH/GSSG signaling did not reflect many of the significant changes *in vivo* (Fig. 3a), Ingenuity Pathway Analysis (IPA, Qiagen) was used to identify NM effects *in vivo*. This analysis confirmed that oxidative stress pathways like glutathione redox reactions I, Nrf2-mediated oxidative stress response, and mitochondrial dysfunction were not among the most significantly enriched pathways (Additional file 2: Fig. S20). In addition, chemokine signaling was found to be mainly enriched in instillation studies with SiO2_7 and SiO2_40 (Fig. 4c). Examples of signaling pathways with higher enrichment included endocytosis signaling, phagosome maturation, leukocyte extravasation signaling, remodeling of epithelial adherens junctions, integrin signaling, and actin cytoskeleton signaling. Apoptosis signaling was again mainly enriched for SiO2_7 and SiO2_40 in the instillation studies, suggesting that these two NMs had the strongest effects. Interestingly, most signaling pathways showed greater enrichment in the recovery groups than in the exposure groups. The complete results of the enrichment analysis can be found in Additional file 1 (Tables E25–E30).

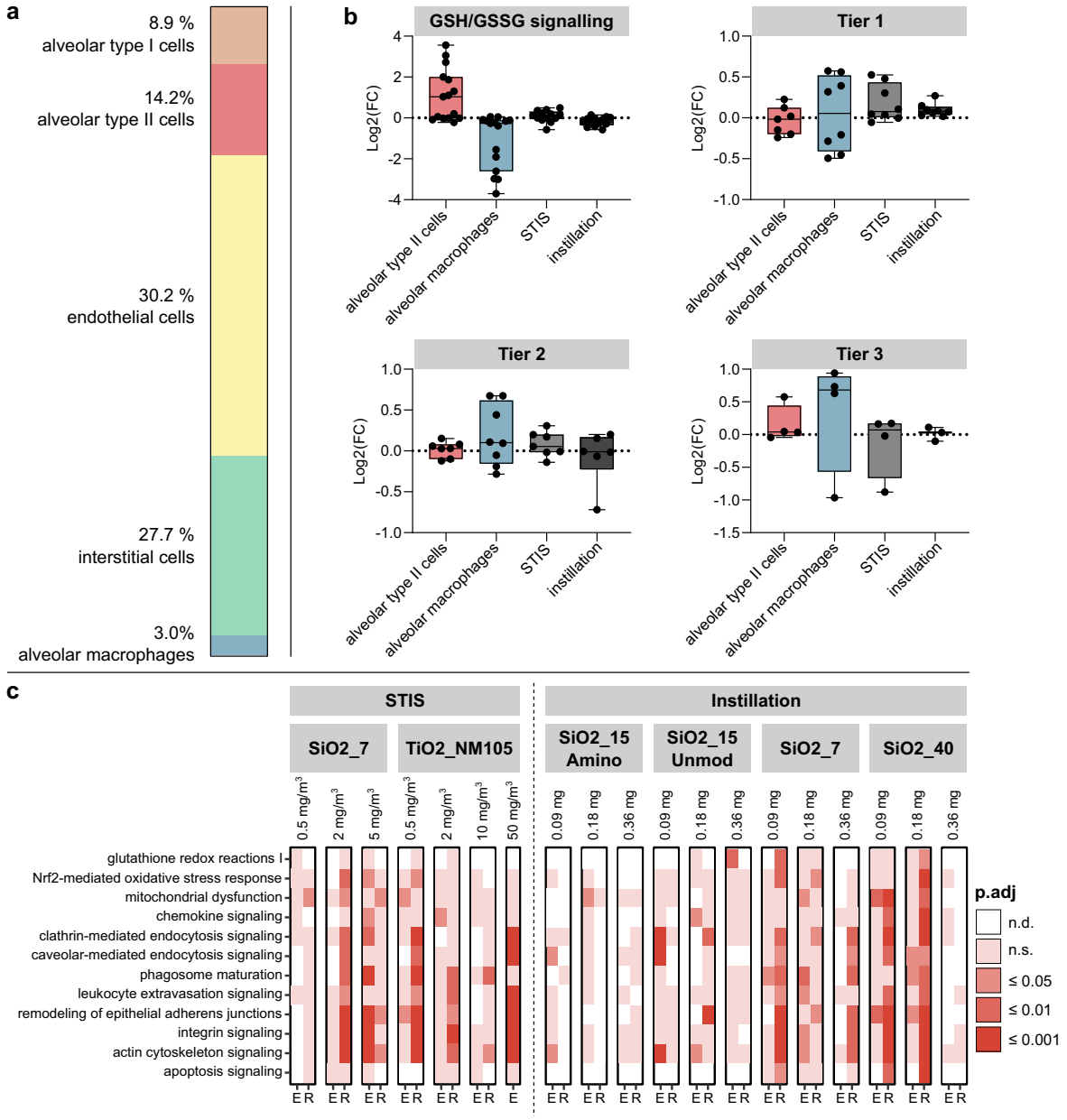


**Fig. 4.** Classification of the *in vivo* results.
Shown is the cellular composition of the rat lung (Crapo et al., 1982) (a), along with Log2(FC) distributions for proteins (Additional file 2: Table S3) and metabolites (Additional file 2: Table S4) associated with GSH/GSSG signaling or the three tiers of oxidative stress. Log2(FC) distributions were compared for alveolar type II cells, alveolar macrophages, STIS, and instillations. For this purpose, the values obtained for SiO2_7 were used because this is the only NM that was evaluated with all four model systems. Thereby, *in vitro* doses of 10 μg/cm$^2$ were selected, whereas *in vivo* exposure group doses of 5 mg/m$^3$ and 0.36 mg were chosen for STIS and instillations, respectively (b). Furthermore, for a selection of IPA pathways, the adjusted *p*-values (p.adj) for enrichment are presented for the *in vivo* studies performed at different doses and for exposure groups (E) and recovery groups (R), distinguishing between *n.d. (not detected), n.s. (not significant, p.adj > 0.05), p.adj ≤ 0.05, p.adj ≤ 0.01, and p.adj ≤ 0.001* (c).

Since SiO2_7 was investigated using STIS and instillations, the results obtained with this NM can be used to compare these two methods, which revealed differences. It is noteworthy that most of the candidates that showed differences were not significantly altered. Exceptions are Txn, Grb2, Glud1, and Vdac1, which were significantly increased in one method and significantly decreased in the other (Fig. 3b). However, at the pathway level, the results of STIS and instillations were largely comparable (Fig. 4c).

### 3.3. Comparison of in vitro and in vivo results

In summary, these results indicate the same classification of NMs *in vitro* and *in vivo*, although the biological effects were different. SiO2_7, SiO2_40, and TiO2_NM105 were classified as “active”, while SiO2_15_Amino led to almost no changes, indicating that it was “passive”. SiO2_15_Unmod resulted in the same trends as SiO2_7 and SiO2_40, suggesting that it may have adverse effects at higher doses.

## 4. Discussion

In the present study, we aimed to analyze the MoAs of a series of five NMs (SiO2_15_Unmod, SiO2_15_Amino, SiO2_7, SiO2_40, and TiO2_NM105) *in vitro* and *in vivo*. We focused on the tiers of oxidative stress (Li et al., 2002; Li et al., 2008; Nel et al., 2006; Xiao et al., 2003) induced in the different model systems by treatment with the NMs at different doses. Alveolar type II cells and alveolar macrophages were used

for *in vitro* toxicity assessment. Both were from rats to ensure comparability with the STIS and instillations performed. Proteomics and metabolomics were used to obtain detailed information on the effects occurring.

### 4.1. Type II cells, macrophages, STIS, and instillations reveal a consistent classification for the NMs investigated here

Based on the significant changes observed, we have attempted to classify the NMs tested here as "active" or "passive". Importantly, SiO2_7 and SiO2_40 were classified as "active" in all four model systems *in vitro* and *in vivo*, confirming our previous classification based on *in vitro* data (Bannuscher et al., 2019; Karkossa et al., 2019). Since SiO2_15_Unmod generally revealed the same trends as SiO2_7 and SiO2_40, albeit with less significance, it should also be classified "active". This is consistent with the literature, where SiO2_15_Unmod has been shown to be "active" *in vitro* (Wiemann et al., 2016) and *in vivo* (Großgarten et al., 2018; Landsiedel et al., 2014). *In vivo*, a mild increase of polymorphonuclear (PMN) neutrophils and lymphocytes has been described after STIS, along with multifocal macrophage aggregates and exacerbation to slight multifocal pulmonary inflammation after the recovery period (Landsiedel et al., 2014). Notably, SiO2_15_Amino was found to be "passive" in all studies conducted, which has also been previously reported *in vitro* and *in vivo* (Karkossa et al., 2019; Landsiedel et al., 2014; Wiemann et al., 2016). This indicates that the surface modification used may influence the effects, as the only difference between SiO2_15_Unmod and SiO2_15_Amino is the amino groups on the surface of the latter, which is in accordance to the literature (Großgarten et al., 2018). Furthermore, this suggests that the route of production may affect NM toxicity, as SiO2_15_Amino and SiO2_15_Unmod, which resulted in fewer effects, are precipitated silica NMs, while SiO2_7 and SiO2_40 are fumed NMs. The observation that fumed NM variants can be more reactive than precipitated ones has been described before as well (Di Cristo et al., 2015), which could be due to the amount of silanol groups on the surface of fumed NMs (Zhang et al., 2012). Reduction of reactive surface silanols has been shown to be effective in decreasing acute pulmonary inflammation and pro-inflammatory effects in macrophages (Sun et al., 2015).

In addition to silica NMs, we also investigated TiO2_NM105. Interestingly, the results of the present study indicated that TiO2_NM105 is "active" in type II cells but "passive" in macrophages, which contrasts with its previous classification as "active" in the same cell line of alveolar macrophages based on the toxicological endpoints LDH, glucuronidase, and tumor necrosis factor (Wiemann et al., 2016). Furthermore, it has been shown to be "active" *in vivo* before (Landsiedel et al., 2014), where it induced an increase in total cell number, PMN neutrophils, monocytes, total protein, glutamyltransferase, LDH, alkaline phosphatase, and *N*-acetyl-β-glucosaminidase based on bronchoalveolar lavage fluids (BALFs), as well as pigment loading of macrophages and mild diffuse histiocytosis, whereas the pulmonary epithelium was not affected. Even after the recovery period, the increases in BALF parameters were not completely reversed. Thus, the macrophages used here possibly underestimated the effects of TiO2_NM105, whereas the type II cells resulted in a classification consistent with previously published data. Of note, the release of LDH, a marker for cytotoxicity in alveolar macrophages, was also considerably lower in the present study (Additional file 2: Table S2) than in the previous study, in which TiO2_NM105 was classified as "active" based on toxicological endpoints (Wiemann et al., 2016). A possible explanation for this observation could be the use of different TiO2_NM105 batches, whereas the experimental setup here was the same. Since the focus of the present study was on oxidative stress, it should be mentioned that the previous study also evaluated ROS release, which did not change in a dose-dependent manner upon treatment with TiO2_NM105. Notably, that study also examined SiO2_15_Amino and SiO2_15_Unmod, of which only SiO2_15_Unmod resulted in significantly altered ROS releases and assignment to "active" NMs (Wiemann et al., 2016), consistent with the data presented here. The fact that differences in oxidative stress formation between the two putatively "active" NMs TiO2_NM105 and SiO2_15_Unmod have already been described in macrophages (Wiemann et al., 2016) and were also observed here, particularly in GSH/GSSG signaling, suggests different MoAs for the two NMs. These results indicate that TiO2_NM105 may not utilize oxidative stress-related signaling pathways in macrophages. However, the observed discrepancy in the classification of TiO2_NM105 highlights that caution should be exercised when classifying NMs, as several factors such as the model system, the experimental setup, and the nature of parameters assessed influence the final classification.

### 4.2. The level of induced oxidative stress varies between type II cells, macrophages, STIS, and instillations

Our main focus was to get mechanistic insights, focusing on the tiers of a previously described stratified model for oxidative stress (Li et al., 2002; Li et al., 2008; Nel et al., 2006; Xiao et al., 2003). Assignment of the observed effects to these tiers revealed that the same NMs can induce different tiers of oxidative stress depending on the model system used.

#### 4.2.1. In type II cells and macrophages, opposite changes were induced by treatment with the putatively "active" NMs

Since the induction of the different tiers of oxidative stress depends mainly on the GSH/GSSG ratio, we first focused on GSH/GSSG signaling. Whereas the putatively "active" NMs resulted in increased abundances of proteins and metabolites related to GSH/GSSG signaling in type II cells, decreased abundances were observed in macrophages. This suggests that type II cells triggered the production of GSH after NM treatment to neutralize the ROS that occurred and thus protect themselves from excessive oxidative stress and further damage, which has been observed previously in type II cells after treatment with different materials (Liu et al., 1996; Stone et al., 1998). In contrast, decreased GSH/GSSG signaling in macrophages suggests decreased GSH levels, which have also been described previously and explained by NM-induced release of GSH or increased requirement for GSH (Boehme et al., 1992; Deneke and Fanburg, 1989). Importantly, the results presented here instead suggest a decreased GSH production.

These opposite effects on GSH/GSSG signaling subsequently led to differences in analytes that can be assigned to the tiers of oxidative stress. Since all proteins required for GSH and NADPH production described here are regulated by Nrf2 (DeNicola et al., 2015; Hayes and Dinkova-Kostova, 2014; Jung and Kwak, 2010; Morales Pantoja et al., 2016), we concluded that in type II cells only tier 1 was affected by NM treatments, but not subsequent tiers. In contrast, in macrophages, significant changes were evident for the "active" NMs across all three tiers.

Differences in the oxidative status of NM-treated cells have already been described for epithelial cells and macrophages, and a depletion of GSH was observed for both cell systems depending on the NM tested. It was hypothesized that either the conversion of GSH to GSSG is responsible for GSH depletion or cell membrane damage leading to GSH leakage (Wang et al., 2014). One possible explanation for the differences in oxidative status between macrophages and epithelial cells upon NM treatment lies in the mechanisms of oxidative stress induction in both. In contrast to epithelial cells, macrophages are known for their ability to induce a respiratory burst during phagocytosis of foreign substances, leading to the production of ROS involved in pathogen killing or degradation. Furthermore, they can act as second messengers and induce pathways related to Nfκb, Ap-1, Mapk, and phosphatidylinositol 3-kinase (Pi3k) (Gwinn and Vallyathan, 2006). Additionally, macrophages bear receptors, *e.g.* Fc receptors, scavenger receptors (SRs), and toll-like receptors (TLRs), that can bind certain types of NMs. For example, recognition of NMs by TLRs and SRs can lead to macrophage activation, triggering inflammatory processes (You et al., 2020). Besides, activation

of TLRs can result in the recruitment of mitochondria to phagosomes and elevated production of mitochondrial ROS (West et al., 2011). Hence, several potential mechanisms are available in macrophages to elicit ROS and subsequent effects, which are not available in epithelial cells, which likely explains the different effects observed in the two cell lines. Differences in the experimental setup may also have influenced the NM-induced effects. Whereas alveolar macrophages were exposed to NMs under serum-free conditions, treatment of alveolar type II cells was performed in presence of serum, affecting surface reactivity, NM uptake, and possibly biological effects.

#### *4.2.2. Not oxidative stress signaling but inflammatory responses were affected in vivo*

While the *in vitro* results allowed the assignment to the tiers of oxidative stress, this concept was not transferable to the *in vivo* results (Fig. 3). This could be because the lung is composed of different cell types (Fig. 4a), which may show different effects upon NM exposure. Another reason could be that the actual deposited doses calculated elsewhere for the experimental setup applied here (Additional file 2: Table S5) (Bannuscher et al., 2020) using the Multiple-Path Particle Dosimetry (MPPD) model (Anjilvel and Asgharian, 1995; Miller et al., 2016), refer to *in vitro* doses that produced little significant change in type II cells and macrophages. However, an enrichment analysis with proteins and metabolites was conducted (Fig. 4c) to provide an overview of affected cellular processes. This revealed that the typical signaling pathways associated with oxidative stress (glutathione redox reactions, Nrf2-mediated oxidative stress response, mitochondrial dysfunction, chemokine signaling, apoptosis signaling) were not among the most significantly enriched signaling pathways. In contrast, signaling pathways related to inflammatory processes, such as endocytosis signaling, phagosome maturation, leukocyte extravasation signaling, remodeling of epithelial adherens junctions, integrin signaling, and actin cytoskeleton signaling, played a major role. In addition, it was observed that the recovery groups exhibited more significant pathway enrichment than the exposure groups, suggesting that NM exposure may lead to long-term effects, which needs to be evaluated in further studies.

Moreover, no clear dose-dependent increase in significantly altered proteins and metabolites was observed after STIS with TiO2_NM105 (Fig. 3a), and the amount of significantly altered proteins and metabolites was comparable to that after treatment with SiO2_7 only at 50 mg/m$^3$ TiO2_NM105, although a NOAEC of 0.5 mg/m$^3$ was described based on STIS with this NM (Landsiedel et al., 2014). In particular, at the 10 mg/m$^3$ tested here, markedly increased numbers of PMN neutrophils, monocytes, total cell counts as well as elevated enzyme and total protein levels were described in that study. Slight elevations were reported already at 2 mg/m$^3$ (Landsiedel et al., 2014). In contrast, a considerable amount of significantly affected proteins and metabolites was observed here only upon exposure with 50 mg/m$^3$, which can be explained by the lung burdens described elsewhere (Bannuscher et al., 2020), which showed considerably lower doses than expected based on the MPPD calculation, especially for the 10 mg/m$^3$ TiO2_NM105. This also explains the inverse dose dependence observed for TiO2_NM105 at the pathway level (Fig. 4c). However, some significantly altered proteins and enriched pathways were already detectable in the exposure and recovery groups of rats exposed to 0.5 mg/m$^3$ TiO2_NM105, although robust significant changes did not occur until 50 mg/m$^3$ TiO2_NM105. Consequently, the desired mechanistic insights were possible anyway with the data described here.

In addition to the differences in the exposure and recovery groups, slight differences were also observed between STIS and instillations performed with SiO2_7. It could be argued that this is due to a divergence of deposited dose in STIS and instillations, but these are comparable. The deposited dose for 5 mg/m$^3$ inhaled SiO2_7 was calculated to be 0.06 μg/cm$^2$ and 0.07 μg/cm$^2$ for the exposure and recovery groups, respectively (Additional file 2: Table S5) (Bannuscher et al., 2020). In contrast, complete deposition of NMs is assumed for instillation. Thus, the applied 0.36 mg SiO2_7 relate to 0.06 μg/cm$^2$ assuming that the rat lung has a surface area of 5571 cm$^2$ (Johanson and Pierce, 1973). Consequently, the observed differences are probably due to the methods themselves and not due to the doses deposited. Notably, the results were comparable at the pathway level, indicating that comparisons on the pathway level are more appropriate when comparing different model systems.

Oxidative DNA damage and protein carbonylation as marker of oxidative stress were also investigated for the rat lung tissues described here (Brandão et al., 2021). Regarding oxidative damage, they found that after instillation only SiO2_7 and SiO2_40 led to oxidative DNA lesions in the exposure groups of each dose tested, which were ameliorated in the recovery groups. In contrast, SiO2_15_Amino led to a slight increase in oxidative DNA damage only at the highest dose tested (0.36 mg) in the recovery group, whereas SiO2_15_Unmod induced no significant changes at all. After inhalations with SiO2_7 and TiO2_NM105, DNA strand breaks were observed for both NMs in the exposure and recovery groups. When they examined protein carbonylation after instillation, they found that SiO2_15_Unmod, SiO2_7, and SiO2_40 had low oxidative potential, while SiO2_15_Amino had medium oxidative potential. In inhalations, SiO2_7 had a medium oxidative potential and TiO2_NM105 had a high oxidative potential. It is also noteworthy that we identified more changes in oxidative stress responses in inhalations compared to instillations (Fig. 4c), although oxidative stress responses were among the most enriched pathways only in the *in vitro* studies we performed and not in the *in vivo* experiments. Thus, these observations are fairly consistent with what we observed, indicating that SiO2_7, SiO2_40, and TiO2_NM105 induce more changes compared to SiO2_15_Amino and SiO2_15_Unmod.

### *4.3. Different mechanisms were triggered in type II cells, macrophages, STIS, and instillations, but the classification of NMs was still consistent*

Taken together, the integrated omics data show that different and even opposite biological responses to the same NM can be detected depending on the *in vitro* model system. Alveolar macrophages appear to be a more sensitive *in vitro* model system as they have shown stronger responses. Therefore, consistent with the 3R concept, they are a valuable tool for acute toxicity testing. Overall, it appears that the *in vitro* models do not adequately reflect the *in vivo* situation. However, it should not be overlooked that a 24 h exposure of selected cell types to NMs cannot reflect what happens in the complex lung after several days of exposure. Signaling pathways can be rapidly turned on or off, and cell types will interact and respond differently. With this in mind, it is important to emphasize that the classification of “active” and “passive” NMs was largely congruent between the model systems tested and also in comparison to previous studies. Omics are thus generally suitable for distinguishing between “active” and “passive” NMs, with the major advantage of providing additional mechanistic insights that cannot be achieved when toxicological endpoints are studied.

## 5. Conclusions

In summary, we show that NM-induced cellular effects can lead to a different assignment to the tiers of oxidative stress, which strongly depends on the model system used. Opposite effects on GSH/GSSG signaling were observed in type II cells and macrophages, with type II cells leading to increased GSH production and thus only to tier 1 and macrophages displaying decreased GSH production and significant changes across all three tiers. Hence, it was not surprising that the assignment was not as clear in the *in vivo* results from rat lung, which consist not only of type II cells and macrophages but also of type I cells, endothelial cells, and interstitial cells. However, the *in vitro* and *in vivo* results were consistent with respect to the classification of the NMs tested, suggesting that both cell lines tested are suitable for the evaluation of NM toxicity. Since macrophages exhibited more significant changes across all

tiers of oxidative stress, they may be a more sensitive model system compared with type II cells. Overall, the results presented highlight that the MoAs of NMs vary in different model systems and, therefore, caution should be exercised when using biomarkers for risk assessment of NMs.

Supplementary data to this article can be found online at https://doi.org/10.1016/j.scitotenv.2021.149538.

## Ethics approval and consent to participate

STIS were conducted under agreement «UN 18 306 DO», approved by the Committee on the Ethics of Animal Experiments of the University of Namur. The experimental design for intratracheal instillation was approved by The Ethics Committee of the "Vasile Goldis" Western University of Arad and authorized by the National Sanitary Veterinary and Food Safety Authority of Romania with registration no. 007/27.11.2017.

## Availability of data and materials

The proteomics and metabolomics data sets generated from alveolar macrophages are available at Zenodo under following DOI: https://doi.org/10.5281/zenodo.3514213.

The proteomics raw data have been deposited to the ProteomeXchange Consortium *via* the PRIDE (Perez-Riverol et al., 2019) partner repository with following data set identifiers: PXD020289 (alveolar type II cells), PXD020158 (alveolar macrophages), PXD020178 (STIS), and PXD020184 (instillations).

## CRediT authorship contribution statement

**Isabel Karkossa:** Methodology, Data curation, Formal analysis, Investigation, Visualization, Writing – original draft, Writing – review & editing. **Anne Bannuscher:** Methodology, Formal analysis, Investigation, Data curation, Writing – review & editing. **Bryan Hellack:** Methodology, Formal analysis, Investigation, Writing – review & editing. **Wendel Wohlleben:** Methodology, Resources, Writing – review & editing. **Julie Laloy:** Methodology, Investigation, Writing – review & editing. **Miruna S. Stan:** Methodology, Investigation, Writing – review & editing. **Anca Dinischiotu:** Resources, Supervision, Writing – review & editing. **Martin Wiemann:** Methodology, Investigation, Resources, Writing – review & editing. **Andreas Luch:** Conceptualization, Resources, Writing – review & editing. **Andrea Haase:** Funding acquisition, Project administration, Conceptualization, Resources, Supervision, Writing – review & editing. **Martin von Bergen:** Funding acquisition, Project administration, Conceptualization, Resources, Supervision, Writing – review & editing. **Kristin Schubert:** Project administration, Conceptualization, Resources, Investigation, Visualization, Supervision, Writing – original draft, Writing – review & editing.

## Declaration of competing interest

The authors declare that they have no known competing financial interests or personal relationships that could have appeared to influence the work reported in this paper.

## Acknowledgements

This project is part of the SIINN ERA-NET and is funded under the ERA-NET scheme of the Seventh Framework Program of the European Commission, BMBF Grant Agreement No. 03XP0008. The STIS performed at the University of Namur were funded by the BfR (grant agreement number 1329-561). Additionally, the authors would like to take this opportunity to thank all institutions and the UFZ-funded ProMetheus platform for proteomics and metabolomics for supporting this project. Furthermore, the authors want to thank Maj Schuster for excellent technical assistance.

## References

Akram, M., 2014. Citric acid cycle and role of its intermediates in metabolism. Cell Biochem. Biophys. 68, 475–478.
Andrieu-Abadie, N., Gouazé, V., Salvayre, R., Levade, T., 2001. Ceramide in apoptosis signaling: relationship with oxidative stress. Free Radic. Biol. Med. 31, 717–728.
Andrieu-Abadie, N., Levade, T., 2002. Sphingomyelin hydrolysis during apoptosis. Biochim. Biophys. Acta Mol. Cell Biol. Lipids 1585, 126–134.
Anjilvel, S., Asgharian, B., 1995. A multiple-path model of particle deposition in the rat lung. Fundam. Appl. Toxicol. 28, 41–50.
Bakand, S., Winder, C., Khalil, C., Hayes, A., 2005. Toxicity assessment of industrial chemicals and airborne contaminants: transition from in vivo to in vitro test methods: a review. Inhal. Toxicol. 17, 775–787.
Bannuscher, A., Hellack, B., Bahl, A., Laloy, J., Herman, H., Stan, M.S., et al., 2020. Metabolomics profiling to investigate nanomaterial toxicity in vitro and in vivo. Nanotoxicology 14, 807–826.
Bannuscher, A., Karkossa, I., Buhs, S., Nollau, P., Kettler, K., Balas, M., et al., 2019. A multi-omics approach reveals mechanisms of nanomaterial toxicity and structure–activity relationships in alveolar macrophages. Nanotoxicology 1–15.
Boehme, D.S., Maples, K.R., Henderson, R.F., 1992. Glutathione release by pulmonary alveolar macrophages in response to particles in vitro. Toxicol. Lett. 60, 53–60.
Brandão, F., Costa, C., Bessa, M.J., Dumortier, E., Debacq-Chainiaux, F., Hubaux, R., et al., 2021. Genotoxicity and gene expression in the rat lung tissue following instillation and inhalation of different variants of amorphous silica nanomaterials (aSiO2 NM). Nanomaterials 11, 1502.
Brookes, P.S., Yoon, Y., Robotham, J.L., Anders, M.W., Sheu, S.-S., 2004. Calcium, ATP, and ROS: a mitochondrial love-hate triangle. Am. J. Physiol. Cell Physiol. 287, C817–C833.
Brunelle, J.K., Letai, A., 2009. Control of mitochondrial apoptosis by the Bcl-2 family. J. Cell Sci. 122, 437–441.
Cohen, G., Hochstein, P., 1963. Glutathione peroxidase: the primary agent for the elimination of hydrogen peroxide in erythrocytes. Biochemistry 2, 1420–1428.
Commission, E., 2012. Types and Uses of Nanomaterials, Including Safety Aspects, Accompanying the Communication From the Commission to the European Parliament, the Council and the European Economic and Social Committee on the Second Regulatory Review on Nanomaterials.
Costa, P.M., Fadeel, B., 2016. Emerging systems biology approaches in nanotoxicology: towards a mechanism-based understanding of nanomaterial hazard and risk. Toxicol. Appl. Pharmacol. 299, 101–111.
Crapo, J.D., Barry, B.E., Gehr, P., Bachofen, M., Weibel, E.R., 1982. Cell number and cell characteristics of the normal human lung. Am. Rev. Respir. Dis. 126, 332–337.
Deneke, S.M., Fanburg, B.L., 1989. Regulation of cellular glutathione. Am. J. Physiol. Lung Cell. Mol. Physiol. 257, L163–L173.
DeNicola, G.M., Chen, P.-H., Mullarky, E., Sudderth, J.A., Hu, Z., Wu, D., et al., 2015. NRF2 regulates serine biosynthesis in non–small cell lung cancer. Nat. Genet. 47, 1475.
Di Cristo, L., Movia, D., Bianchi, M.G., Allegri, M., Mohamed, B.M., Bell, A.P., et al., 2015. Pro-inflammatory effects of pyrogenic and precipitated amorphous silica nanoparticles in innate immunity cells. Toxicol. Sci. 150, 40–53.
Dickinson, D.A., Forman, H.J., 2002. Cellular glutathione and thiols metabolism. Biochem. Pharmacol. 64, 1019–1026.
Domachowske, J.B., Bonville, C.A., Gao, J.-L., Murphy, P.M., Easton, A.J., Rosenberg, H.F., 2000. The chemokine macrophage-inflammatory protein-1a and its receptor CCR1 control pulmonary inflammation and antiviral host defense in paramyxovirus infection. J. Immunol. 165, 2677–2682.
Driessen, M.D., Mues, S., Vennemann, A., Hellack, B., Bannuscher, A., Vimalakanthan, V., et al., 2015. Proteomic analysis of protein carbonylation: a useful tool to unravel nanoparticle toxicity mechanisms. Part. Fibre Toxicol. 12, 36.
Driscoll, K.E., Costa, D.L., Hatch, G., Henderson, R., Oberdorster, G., Salem, H., et al., 2000. Intratracheal instillation as an exposure technique for the evaluation of respiratory tract toxicity: uses and limitations. Toxicol. Sci. 55, 24–35.
Fröhlich, E., Salar-Behzadi, S., 2014. Toxicological assessment of inhaled nanoparticles: role of in vivo, ex vivo, in vitro, and in silico studies. Int. J. Mol. Sci. 15, 4795–4822.
Fubini, B., Hubbard, A., 2003. Reactive oxygen species (ROS) and reactive nitrogen species (RNS) generation by silica in inflammation and fibrosis. Free Radic. Biol. Med. 34, 1507–1516.
Geiser, M., 2002. Morphological aspects of particle uptake by lung phagocytes. Microsc. Res. Tech. 57, 512–522.
Geiser, M., Kreyling, W.G., 2010. Deposition and biokinetics of inhaled nanoparticles. Part. Fibre Toxicol. 7, 2.
Gobin, S.J., Biesta, P., Van den Elsen, P.J., 2003. Regulation of human beta 2-microglobulin transactivation in hematopoietic cells. Blood 101, 3058–3064.
Graffelman, J., 2019. Calibrate: Calibration of Scatterplot and Biplot Axes. R package version 1.7.5.
Grandjean-Laquerriere, A., Antonicelli, F., Gangloff, S.C., Guenounou, M., Le Naour, R., 2007. UVB-induced IL-18 production in human keratinocyte cell line NCTC 2544 through NF-kappaB activation. Cytokine 37, 76–83.
Großgarten, M., Holzlechner, M., Vennemann, A., Balbekova, A., Wieland, K., Sperling, M., et al., 2018. Phosphonate coating of SiO2 nanoparticles abrogates inflammatory effects and local changes of the lipid composition in the rat lung: a complementary bioimaging study. Part. Fibre Toxicol. 15, 31.
Gu, Z., Gu, L., Eils, R., Schlesner, M., Brors, B., 2014. Circlize implements and enhances circular visualization in R. Bioinformatics 30, 2811–2812.
Gwinn, M.R., Vallyathan, V., 2006. Respiratory burst: role in signal transduction in alveolar macrophages. J. Toxicol. Environ. Health Part B 9, 27–39.
Haase, A., Dommershausen, N., Schulz, M., Landsiedel, R., Reichardt, P., Krause, B.-C., et al., 2017. Genotoxicity testing of different surface-functionalized SiO2, ZrO2 and silver nanomaterials in 3D human bronchial models. Arch. Toxicol. 91.

Hayes, J.D., Dinkova-Kostova, A.T., 2014. The Nrf2 regulatory network provides an interface between redox and intermediary metabolism. Trends Biochem. Sci. 39, 199–218.
Holden, P.A., Klaessig, F., Turco, R.F., Priester, J.H., Rico, C.M., Avila-Arias, H., et al., 2014. Evaluation of exposure concentrations used in assessing manufactured nanomaterial environmental hazards: are they relevant? Environ. Sci. Technol. 48, 10541–10551.
Huang, C., Yao, J.Y., Li, Z.F., Liu, L.Y., Ni, L., Song, T.S., 2007. Small interfering RNA-mediated nuclear factor-kappaB P65 suppression induces apoptosis of hepatic carcinoma SMMC-7721 cells. J. South. Med. Univ. 27, 1841–1844.
Huang, Y.-W., Wu, C.-h., Aronstam, R.S., 2010. Toxicity of transition metal oxide nanoparticles: recent insights from in vitro studies. Materials 3, 4842–4859.
Hughes, C.S., Foehr, S., Garfield, D.A., Furlong, E.E., Steinmetz, L.M., Krijgsveld, J., 2014. Ultrasensitive proteome analysis using paramagnetic bead technology. Mol. Syst. Biol. 10, 757.
Hughes, C.S., Moggridge, S., Muller, T., Sorensen, P.H., Morin, G.B., Krijgsveld, J., 2019. Single-pot, solid-phase-enhanced sample preparation for proteomics experiments. Nat. Protoc. 14, 68–85.
Johanson Jr., W.G., Pierce, A.K., 1973. Lung structure and function with age in normal rats and rats with papain emphysema. J. Clin. Invest. 52, 2921–2927.
Jung, K.-A., Kwak, M.-K., 2010. The Nrf2 system as a potential target for the development of indirect antioxidants. Molecules 15, 7266–7291.
Kanehisa, M., 2019. Toward understanding the origin and evolution of cellular organisms. Protein Sci. 28, 1947–1951.
Kanehisa, M., Goto, S., 2000. KEGG: Kyoto encyclopedia of genes and genomes. Nucleic Acids Res. 28, 27–30.
Kanehisa, M., Sato, Y., Furumichi, M., Morishima, K., Tanabe, M., 2019. New approach for understanding genome variations in KEGG. Nucleic Acids Res. 47, D590–d595.
Karkossa, I., Bannuscher, A., Hellack, B., Bahl, A., Buhs, S., Nollau, P., et al., 2019. An in-depth multi-omics analysis in RLE-6TN rat alveolar epithelial cells allows for nanomaterial categorization. Part. Fibre Toxicol. 16, 38.
Keller, A.A., McFerran, S., Lazareva, A., Suh, S., 2013. Global life cycle releases of engineered nanomaterials. J. Nanopart. Res. 15, 1692.
Kim, S.M., Lee, S.Y., Cho, J.S., Son, S.M., Choi, S.S., Yun, Y.P., et al., 2010. Combination of ginsenoside Rg3 with docetaxel enhances the susceptibility of prostate cancer cells via inhibition of NF-kappaB. Eur. J. Pharmacol. 631, 1–9.
Ko, J., Yun, C.Y., Lee, J.S., Kim, J.H., Kim, I.S., 2007. p38 MAPK and ERK activation by 9-cis-retinoic acid induces chemokine receptors CCR1 and CCR2 expression in human monocytic THP-1 cells. Exp. Mol. Med. 39, 129–138.
Krämer, A., Green, J., Pollard Jr., J., Tugendreich, S., 2013. Causal analysis approaches in ingenuity pathway analysis. Bioinformatics 30, 523–530.
Krebs, H.A., 1970. The history of the tricarboxylic acid cycle. Perspect. Biol. Med. 14, 154–170.
Kreyling, W.G., Hirn, S., Schleh, C., 2010. Nanoparticles in the lung. Nat. Biotechnol. 28, 1275–1276.
Kreyling, W.G., Semmler-Behnke, M., Takenaka, S., Moller, W., 2013. Differences in the biokinetics of inhaled nano- versus micrometer-sized particles. Acc. Chem. Res. 46, 714–722.
Kreyling, W.G., Semmler, M., Erbe, F., Mayer, P., Takenaka, S., Schulz, H., et al., 2002. Translocation of ultrafine insoluble iridium particles from lung epithelium to extrapulmonary organs is size dependent but very low. J. Toxic. Environ. Health A 65, 1513–1530.
Landsiedel, R., Ma-Hock, L., Hofmann, T., Wiemann, M., Strauss, V., Treumann, S., et al., 2014. Application of short-term inhalation studies to assess the inhalation toxicity of nanomaterials. Part. Fibre Toxicol. 11, 16.
Lee, I.T., Yang, C.M., 2013. Inflammatory signalings involved in airway and pulmonary diseases. Mediat. Inflamm. 2013, 791231.
Li, K., Wei, L., Huang, Y., Wu, Y., Su, M., Pang, X., et al., 2016. Leptin promotes breast cancer cell migration and invasion via IL-18 expression and secretion. Int. J. Oncol. 48, 2479–2487.
Li, N., Kim, S., Wang, M., Froines, J., Sioutas, C., Nel, A., 2002. Use of a stratified oxidative stress model to study the biological effects of ambient concentrated and diesel exhaust particulate matter. Inhal. Toxicol. 14, 459–486.
Li, N., Xia, T., Nel, A.E., 2008. The role of oxidative stress in ambient particulate matter-induced lung diseases and its implications in the toxicity of engineered nanoparticles. Free Radic. Biol. Med. 44, 1689–1699.
Liu, R.-M., Hu, H., Robison, T.W., Forman, H.J., 1996. Increased gamma-glutamylcysteine synthetase and gamma-glutamyl transpeptidase activities enhance resistance of rat lung epithelial L2 cells to quinone toxicity. Am. J. Respir. Cell Mol. Biol. 14, 192–197.
Madesh, M., Hajnóczky, G., 2001. VDAC-dependent permeabilization of the outer mitochondrial membrane by superoxide induces rapid and massive cytochrome. J. Cell Biol. 155, 1003–1016.
Mahto, A., 2018. splitstackshape: Stack and Reshape Datasets After Splitting concatenated values.
Manke, A., Wang, L., Rojanasakul, Y., 2013. Mechanisms of nanoparticle-induced oxidative stress and toxicity. Biomed. Res. Int. 2013, 15.
Meister, A., Anderson, M.E., 1983. Glutathione. Annu. Rev. Biochem. 52, 711–760.
Mendoza, R.P., Brown, J.M., 2019. Engineered nanomaterials and oxidative stress: current understanding and future challenges. Curr. Opin. Toxicol. 13, 74–80.
Miao, L., St Clair, D.K., 2009. Regulation of superoxide dismutase genes: implications in disease. Free Radic. Biol. Med. 47, 344–356.
Miller, F.J., Asgharian, B., Schroeter, J.D., Price, O., 2016. Improvements and additions to the multiple path particle dosimetry model. J. Aerosol Sci. 99, 14–26.
Morales Pantoja, I.E., Hu, C.-l., Perrone-Bizzozero, N.I., Zheng, J., Bizzozero, O.A., 2016. Nrf2-dysregulation correlates with reduced synthesis and low glutathione levels in experimental autoimmune encephalomyelitis. J. Neurochem. 139, 640–650.
Morimoto, Y., Izumi, H., Yoshiura, Y., Tomonaga, T., Lee, B.-W., Okada, T., et al., 2016. Comparison of pulmonary inflammatory responses following intratracheal instillation and inhalation of nanoparticles. Nanotoxicology 10, 607–618.
Muhlfeld, C., Rothen-Rutishauser, B., Blank, F., Vanhecke, D., Ochs, M., Gehr, P., 2008. Interactions of nanoparticles with pulmonary structures and cellular responses. Am. J. Physiol. Lung Cell. Mol. Physiol. 294, L817-29.
Nel, A., Xia, T., Mädler, L., Li, N., 2006. Toxic potential of materials at the nanolevel. Science 311, 622–627.
Neuwirth, E., 2014. ColorBrewer Palettes, pp. 1.1–2.
Niture, S., Ramalinga, M., Kedir, H., Patacsil, D., Niture, S.S., Li, J., et al., 2018. TNFAIP8 promotes prostate cancer cell survival by inducing autophagy. Oncotarget 9, 26884–26899.
Oberdörster, G., Oberdörster, E., Oberdörster, J., 2005. Nanotoxicology: an emerging discipline evolving from studies of ultrafine particles. Environ. Health Perspect. 113, 823–839.
OECD, 2012. Proposal for a Template and Guidance on Developing and Assessing the Completeness of Adverse Outcome Pathways.
OECD, 2018. Report on considerations from case studies on Integrated Approaches for Testing and Assessment (IATA), ENV/JM/MONO(2018)25. Series on Testing and Assessment No. 289. ENV/JM/MONO(2018)25.
Pajares, M., Rojo, A.I., Arias, E., Díaz-Carretero, A., Cuervo, A.M., Cuadrado, A., 2018. Transcription factor NFE2L2/NRF2 modulates chaperone-mediated autophagy through the regulation of LAMP2A. Autophagy 14, 1310–1322.
Perez-Riverol, Y., Csordas, A., Bai, J., Bernal-Llinares, M., Hewapathirana, S., Kundu, D.J., et al., 2019. The PRIDE database and related tools and resources in 2019: improving support for quantification data. Nucleic Acids Res. 47, D442–d450.
Piccinno, F., Gottschalk, F., Seeger, S., Nowack, B., 2012. Industrial production quantities and uses of ten engineered nanomaterials in Europe and the world. J. Nanopart. Res. 14, 1109.
Potratz, S., Tarnow, P., Jungnickel, H., Baumann, S., von Bergen, M., Tralau, T., et al., 2017. Combination of metabolomics with cellular assays reveals new biomarkers and mechanistic insights on xenoestrogenic exposures in MCF-7 cells. Chem. Res. Toxicol. 30, 4, 883–892.
Qiagen. Ingenuity Pathway Analysis.
Rahman, I., MacNee, W., 1998. Role of transcription factors in inflammatory lung diseases. Thorax 53, 601–612.
Richman, P., Meister, A., 1975. Regulation of gamma-glutamyl-cysteine synthetase by nonallosteric feedback inhibition by glutathione. J. Biol. Chem. 250, 1422–1426.
Risom, L., Møller, P., Loft, S., 2005. Oxidative stress-induced DNA damage by particulate air pollution. Mutat. Res. 592, 119–137.
Sawada, R., Jardine, K.A., Fukuda, M., 1993. The genes of major lysosomal membrane glycoproteins, lamp-1 and lamp-2. 5'-flanking sequence of lamp-2 gene and comparison of exon organization in two genes. J. Biol. Chem. 268, 9014–9022.
Semmler-Behnke, M., Takenaka, S., Fertsch, S., Wenk, A., Seitz, J., Mayer, P., et al., 2007. Efficient elimination of inhaled nanoparticles from the alveolar region: evidence for interstitial uptake and subsequent reentrainment onto airways epithelium. Environ. Health Perspect. 115, 728–733.
Semmler, M., Seitz, J., Erbe, F., Mayer, P., Heyder, J., Oberdörster, G., et al., 2004. Long-term clearance kinetics of inhaled ultrafine insoluble iridium particles from the rat lung, including transient translocation into secondary organs. Inhal. Toxicol. 16, 453–459.
Sies H. Oxidative stress: Introduction in oxidative stress: In oxidative stress: oxidative stress: oxidants and antioxidant ed Sies H. 19191; pp xv-xxiv. Academic press London.
Spiess, A.N., 2018. qpcR: Modelling and Analysis of Real-Time PCR Data. R package v. 1.4-1.
Stark, W.J., Stoessel, P.R., Wohlleben, W., Hafner, A., 2015. Industrial applications of nanoparticles. Chem. Soc. Rev. 44, 5793–5805.
Steuer, A.E., Brockbals, L., Kraemer, T., 2019. Metabolomic strategies in biomarker research-new approach for indirect identification of drug consumption and sample manipulation in clinical and forensic toxicology? Front. Chem. 7, 319.
Stone, V., Miller, M.R., Clift, M.J.D., Elder, A., Mills, N.L., Moller, P., et al., 2017. Nanomaterials versus ambient ultrafine particles: an opportunity to exchange toxicology knowledge. Environ. Health Perspect. 125, 106002.
Stone, V., Shaw, J., Brown, D.M., MacNee, W., Faux, S.P., Donaldson, K., 1998. The role of oxidative stress in the prolonged inhibitory effect of ultrafine carbon black on epithelial cell function. Toxicol. in Vitro 12, 649–659.
Sun, B., Pokhrel, S., Dunphy, D.R., Zhang, H., Ji, Z., Wang, X., et al., 2015. Reduction of acute inflammatory effects of Fumed silica nanoparticles in the lung by adjusting silanol display through calcination and metal doping. ACS Nano 9, 9357–9372.
Taurozzi, J.S., Hackley, V.A., Wiesner, M.R., 2011. Ultrasonic dispersion of nanoparticles for environmental, health and safety assessment–issues and recommendations. Nanotoxicology 5, 711–729.
Thompson, A., Schafer, J., Kuhn, K., Kienle, S., Schwarz, J., Schmidt, G., et al., 2003. Tandem mass tags: a novel quantification strategy for comparative analysis of complex protein mixtures by MS/MS. Anal. Chem. 75, 1895–1904.
Wang, L., Pal, A.K., Isaacs, J.A., Bello, D., Carrier, R.L., 2014. Nanomaterial induction of oxidative stress in lung epithelial cells and macrophages. J. Nanopart. Res. 16, 2591.
Wang, Z., Karkossa, I., Großkopf, H., Rolle-Kampczyk, U., Hackermüller, J., von Bergen, M., et al., 2021. Comparison of quantitation methods in proteomics to define relevant toxicological information on AhR activation of HepG2 cells by BaP. Toxicology 448, 152652.
Warnes, G.R., Bolker, B., Bonebakker, L., Gentleman, R., Liaw, W.H.A., Lumley, T., et al., 2016. gplots: Various R Programming Tools for Plotting Data.
West, A.P., Brodsky, I.E., Rahner, C., Woo, D.K., Erdjument-Bromage, H., Tempst, P., et al., 2011. TLR signalling augments macrophage bactericidal activity through mitochondrial ROS. Nature 472, 476–480.

Wewering, F., Jouy, F., Wissenbach, D.K., Gebauer, S., Blüher, M., Gebhardt, R., et al., 2016. Characterization of chemical-induced sterile inflammation in vitro: application of the model compound ketoconazole in a human hepatic co-culture system. Arch. Toxicol. 1–12.
Wickham, H., 2011. The split-apply-combine strategy for data analysis. J. Stat. Softw. 40, 1–29.
Wickham, H., 2016. ggplot2: Elegant Graphics for Data Analysis. Springer-Verlag, New York.
Wickham, H., Bryan, J., 2018. readxl: Read Excel Files.
Wickham, H., Henry, L., 2018. tidyr: easily tidy data with "spread ()" and "gather ()" functions. R package version 0.8. 0. 2018.
Wiemann, M., Vennemann, A., Sauer, U.G., Wiench, K., Ma-Hock, L., Landsiedel, R., 2016. An in vitro alveolar macrophage assay for predicting the short-term inhalation toxicity of nanomaterials. J. Nanobiotechnol. 14, 16.
Wiemann, M., Vennemann, A., Stintz, M., Retamal Marin, R.R., Babick, F., Lindner, G.G., et al., 2018. Effects of ultrasonic dispersion energy on the preparation of amorphous SiO (2) nanomaterials for in vitro toxicity testing. Nanomaterials 9.
Wishart, D.S., 2016. Emerging applications of metabolomics in drug discovery and precision medicine. Nat. Rev. Drug Discov. 15, 473–484.
Xiao, G.G., Wang, M., Li, N., Loo, J.A., Nel, A.E., 2003. Use of proteomics to demonstrate a hierarchical oxidative stress response to diesel exhaust particle chemicals in a macrophage cell line. J. Biol. Chem. 278, 50781–50790.
Yang, Y., Wu, J., Wang, J., 2016. A database and functional annotation of NF-?B target genes. Int. J. Clin. Exp. Med. 9, 7986–7995.
You, D.J., Lee, H.Y., Bonner, J.C., 2020. Macrophages: first innate immune responders to nanomaterials. In: Bonner, J.C., Brown, J.M. (Eds.), Interaction of Nanomaterials With the Immune System. Springer International Publishing, Cham, pp. 15–34.
Zhang, H., Dunphy, D.R., Jiang, X., Meng, H., Sun, B., Tarn, D., et al., 2012. Processing pathway dependence of amorphous silica nanoparticle toxicity: colloidal vs pyrolytic. J. Am. Chem. Soc. 134, 15790–15804.